2016

Dropwise condensation detection in a single image

Tarik Loukili
Iowa State University

Dropwise condensation detection in a single image

by

Tarik Loukili

A thesis submitted to the graduate faculty

in partial fulfillment of the requirements for the degree of

MASTER OF SCIENCE

Major: Electrical Engineering (Communications and Signal Processing)

Program of Study Committee:

Timothy Bigelow, Major Professor
Santosh Pandey
Wang Zhendago

The student author, whose presentation of the scholarship herein was approved by the program of study committee, is solely responsible for the content of this thesis. The Graduate College will ensure this thesis is globally accessible and will not permit alterations after a degree is conferred.

Iowa State University

Ames, Iowa

2017

TABLE OF CONTENTS

Page

LIST OF FIGURES

Page

LIST OF ACRONYMS AND ABBREVIATIONS

CNN:	convolutional neural network
COC	circle of confusion
CV	computer vision
FFT	fast Fourier transform
FOV	field of view
OOF	out of focus
ROI	region of interest
SVM	support vector machine

ACKNOWLEDGMENTS

I would like to thank my collegue at John Deere, Shayne Rich, for his support and help in builidng the Fog-Lab. Special thanks to the Lamda Reseach Group engineering staff, especially Dave Jacobson and Michael Gauvin for their help with the TracePro free trial and technical support.

I would also like to thank my major professor Dr. Timothy Bigelow, for his guidance and valuable feedback. I am grateful he kept me focused and on track, preventing me from getting lost in the weeds somewhere between physics and engineering.

.

ABSTRACT

The detection of dropwise condensation in the camera field is a complex problem that requires an interdisciplinary approach in order to build an accurate model for image formation. In the current work, the effect of dropwise condensation at the microscopic level was analyzed using geometrical optics and optical simulation. The results showed that pixels from a region within the foggy image area will tend to move toward the center of this patch in the RGB space. The results also showed a loss in high frequencies of the image patch. Based on these findings, a method was developed to detect condensation from a single image using local gradient magnitude as a texture feature combined with the dispersion of pixel color information in the RGB space. This approach segments the image into clear and foggy regions using a clustering algorithm (Expectation Maximization). The misclassified patches are corrected in a second pass using the probability of neighboring patches to be foggy.

The algorithm was successful using data collected by a Fog-Lab that was designed and built to capture images in a controlled environment at different condensation levels. This work is presumed to be the first that addresses condensation detection from a single image at early stages.

CHAPTER 1. INTRODUCTION

One of the main challenges of visual detection of condensation on a glass or a camera lens is the complexity of modelling, simulating or even reproducing the same exact phenomena. When the light that is reflected by objects in a scene travels toward the camera sensor and passes through glass with partial or total condensation, it undergoes many alterations giving the captured image a blurry or hazy look. A simple blur detection approach to recognize the moisture build-up is inadequate because there are multiple levels of degradations. When light traverses a water droplet some of it will be reflected causing information loss and some of it will be refracted; thus, some may land in the wrong spot of the image whereas some will be transmitted as normal. The glass holding the suspended water droplets is located between the camera sensor and the viewing scene which causes the image to be out of focus. To further compound the problem, the droplets are distributed in a non-uniform fashion making it impossible to model the phenomena using an invariant blur kernel. In addition, the image sampling process at the camera sensor level produce a down-sampled image where each pixel contains information for a region of the viewing scene as well as one or many water droplets depending on the size of the droplet and the distance between the glass and the camera sensor.

The existing work that examines detection of water condensation ([12], [13], [14], [15], [16], [17], [18], [19], [20], [21], [22]) is based on the assumption that the droplet is visually recognizable in the image which means that its diameter is many pixels in width. This is not always the case as condensation goes through multiple stages before reaching the phase where a single droplet becomes large enough to be distinguishable. In this study condensation process is described first from the nano-scale to the macro-scale state, and the characteristics are described for each stage as well as proposed models for image formation in the presence of condensation. Then a simulation (TracePro) is used to

develop an understanding of the impact of the droplet's shape, size and density on the transmissibility of light in the presence of condensation. Next, a description is provided of the Condensation-Lab-Box that was built in this work for data collection. The Lab-Box enabled the capture of images with moisture built-up in a controlled environment. Finally, a discussion is provided regarding the information and insight developed previously to analyze images and use specific features to detect condensation reliablably.

CHAPTER 2. RELATED WORK

The effect of condensation on vision systems has been previously explored only at the final stages, when a water droplet reaches a size that is large enough to make it a distinguishable feature that is visible within a captured image. Related prior work is discussed as follows.

2.1 Machine Learning Approach

Machot et al. [17] and Eigen et al. [18] used a convolution neural network to detect water droplets. In their work, the image is divided into patches where each one is classified as either clean or occluded by the droplet. The authors claimed that the algorithm was able to detect the affected patches except when the droplet was very heavy. Webster and Breckon [16] used a set of shape, texture and color features to train a classifier for Raindrop detection using SVM and Random Forest. Kurishata et al. [20] used PCA on a droplet patch to produce a template (eigendrops) during the training phase, and then performed cross correlation to make an identification. This approach seems to perform poorly whenever the sky is not included in the scene, which implies that the eigendrops depend highly on the training set.

2.2 Photometric Approach

Halimeh and Roser [19] derived a rain drop photometric model using geometrical optic laws which enabled them to distinguish the image captured by the droplet from a clear image. A limitations of this method is the assumption that the droplet is big enough to contain a minimum amount of textures. It is also assumed that the droplet is not out of focus which is not the case in most examples. For this approach to work, each droplet requires a clear image region to find corresponding pixels.

2.3 Spatio-Temporal Approaches

You et al. [21] used a stream of images to detect regions with a circular shape, where the intensity does not change much and the pixel motion intra-frame is slow. This method assumes that the background is changing. The approach fails for pixels inside the droplet because the scene changes, which also implies the intensity of the droplet pixels will also change. This is apparent from results using intensity features where only the edges of the droplets are detected because the light hitting near the edges of the droplet undergo losses due to reflection making the edges appear darker in all frames. Nashashibi et al. [22] used a similar concept but monitored the edges within the droplet as a metric for blurriness.

From the nucleation of the droplet at the nano-scale all the way until the droplet reaches the size of a few pixels it is impossible to use the aforementioned techniques. The active work targeting these stages only focuses on the light transmission through condensation for non-vision applications (e.g. the effect of condensation on light transmittance into greenhouses).

CHAPTER 3. EXPERIMENTAL SET-UP AND DATA COLLECTION

A Fog-Lab was designed and built to collect data with Ground-Truth. The Lab enabled us to capture images in a controlled environment with different levels of condensation. The Lab contain three main systems: an imaging system, a micro-verification system, and a fog chamber.

3.1 Fog-Lab

3.1.1 Imaging system

An IDS uEYE 1220LE camera with a CMOS sensor, a global shutter that is able to capture up to 87.2 fps, was used to take images with a resolution of 752 × 480 and a pixel size of 6 µm. The lens used was a Tamron 1/1.8 image with an 8 mm focal length, whose angle of view is 50.8"×38.6" and can be focused from 10 cm to infinity. The camera was placed on a moveable mount to enable the user to slide it either closer or further away from the chamber window (Figure 3.1).

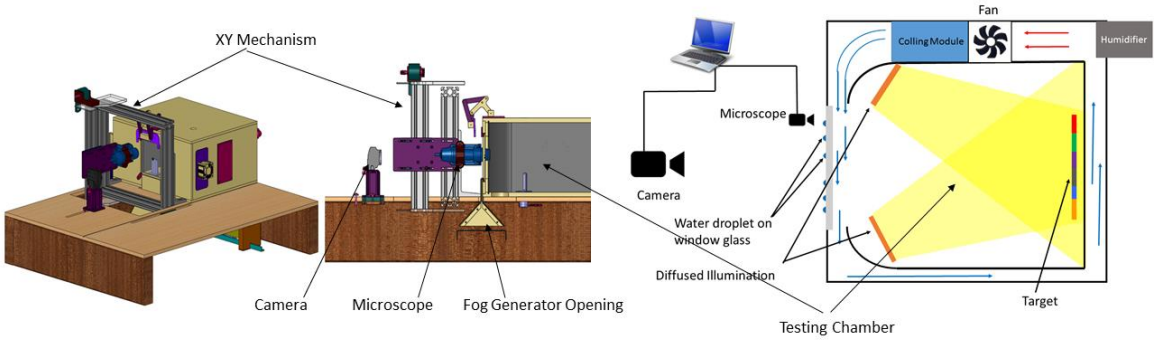

Figure 3.1. Fog-Lab

3.1.2 Micro-Verification System

In order to provide verification at the microscopic level, a USB microscope with a resolution of 1280 ×960 and a 200 magnification was placed 5 mm from the chamber window to enable monitoring of droplet growth with a diameter from 50 µm to a couple

of millimeters. The microscope included a GUI application that enabled the user to take droplet measurement, video, and snapshot captures. The microscope was mounted on an XY mechanism to scan the window by moving the microscope using a predefined speed/step in a horizontal and vertical axis.

3.1.3 Fog Chamber

The Fog-Chamber is a 29cm × 34cm × 16cm insulating box. A channel allows the circulation of the air through a cooling element, and forces the cool air to flow in front of the glass window. A sensor placed inside the channel measures the inside temperature to assist in determining the appropriate time to start generating the fog. Inside the chamber a set of LEDs are placed in such a way to generate a diffused light, to provide uniform illumination and avoid an image with hot spots. The target is placed on the back of the box and is accessible through a rotating door.

3.2 Data Collection

A few steps in the data collection process (e.g the microscope scanning through the window glass and capturing images) in order to increase the accuracy of the data collected. First, the illumination inside the box was calibrated. A Matlab script was developed to automatically acquire the images captured by the IDS camera and visualize the illumination distribution in the image space (Figure 3.2).

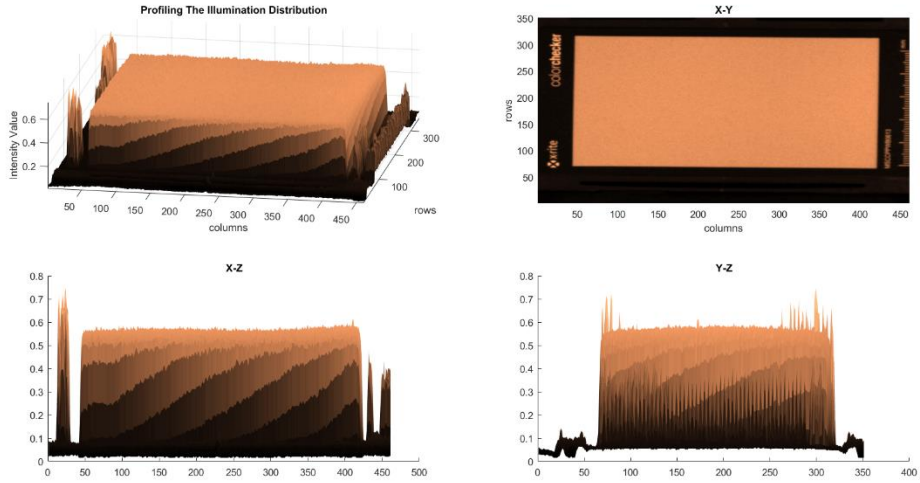

Figure 3.2. A white target used to calibrate the chamber illumination

After ensuring that the illumination is uniform across the image plan, the white target was swapped with the appropriate target of choice, and then the box was closed. Fans were used to power the cooling element and force the air flow in front of the glass. This cooled the glass, thus allowing condensation of vapor and preventing fast evaporation which can occur at room temperature. Once the temperature dropped below 12 C^o we started the fog generator (a Facial Steamer was used in this study). Steam was collected and guided through a cone to a flat collector that forces a thin film of vapor to flow in front of the glass. The fog flow was interrupted at specific intervals to allow for capturing images by the IDS camera. Microscopic images were taken of the condensation region.

CHAPTER 4. SIMULATION

A ray tracing analysis was performed of the light transmission through single and multiple droplets of varying contact angles and droplet densities on a glass slab. This was done to verify the formulas that were derived and explained in this research (Models for condensation stages) relating to the droplet contact angle with the diameter of the circle of confusion.

The software used was TracePro which is an optical engineering software that allows the user to design, analyze and simulate optical and illumination systems. The package developed by Lambda Research Corporation is very powerful but requires a learning phase.

4.1 Single Droplet

First, a single droplet on a glass slab was designed, with the droplet base diameter (the base is the droplet side in contact with the glass surface) maintained constant while varying the contact angle. A uniform parallel light ray with a wave length of 550 nm strikes the substrate surface on the dry side at 90 degrees, the droplet diameter is 500 µm and a collecting element is placed 25 cm away from the glass substrate (Figure 4.1).

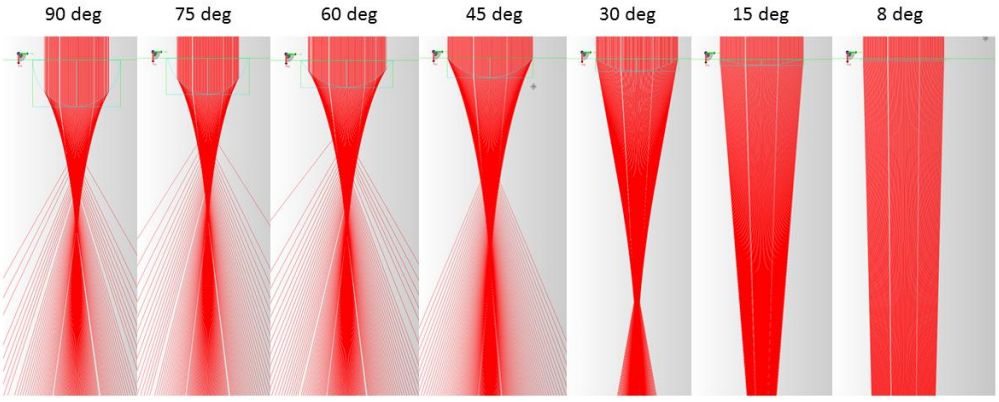

Figure 4.1. Single droplet ray tracing

Two interesting observations were made druing this first simulation. When the contact angle was very low (due to filmwise condensation), the scattering of light is negligible. As the contact angle gets larger the back focal length becames closer to the droplet base. Beyond a certain contact angle rays were lost near the edges of the droplet due to reflection (see Appendix A-1 and A-2).

4.2 Multiple Droplets

The random nucleation process was simulated to generate multiple droplets. A Matlab simulation was developed to take the droplet's initial and maximum size, contact angle, the condensation window size and the droplet's densities (coverage area percentages) to generate multiple droplet distribution maps (a map for each droplet's density). These were used in turn to generate texture files that could be used within TracePro to model the droplets at their specific locations on a glass substrate. Then we selected the illumination source to be similar to the one used in the single droplet simulation, except this time the illumination field area matched the size of the glass window. Figure 4.2 illustrates the pipeline developed and used to simulate the effect of condensation at multiple stages. The glass substrate size is 5cm ×5cm (the red square depicts the irradiance map).

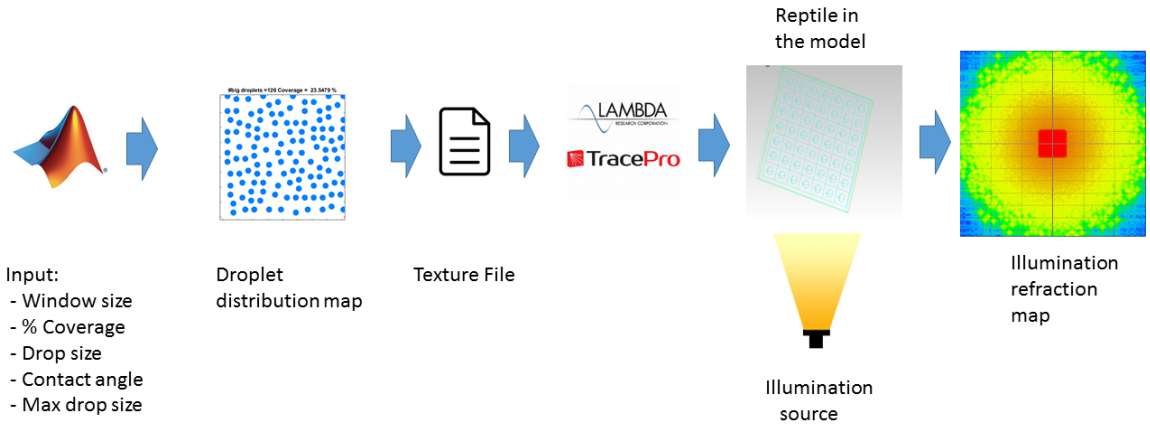

Figure 4.2. Simulation pipeline

The simulation results are summarized in Figure 4.3, where the columns represent the coverage area (droplets density) and the rows are for the selected contact angles. The top row shows the distribution maps generated by the Matlab script while the other rows shows the irradiance map at the collecting element placed 25 cm from the glass surface.

It became apparent that the condensation scatters the light. A portion of this light was not affected and reached its normal destination. This is mainly the case for light rays penetrating the slab at the clear areas (between droplets) and those hitting each droplet near its center as they will undergo the minimum refraction. The other part will be refracted making the active region (area that received the light rays) at the collection plan much larger than the window size. The size of this active region is the same regardless of the droplet density but the irradiance distribution within this region change based on the coverage area (density). As the number of droplets increases, concentric regions appeared with different irradiances around the window size. When the contact angle increased beyond a threshold value a percentage of the emitted light was reflected and never made it through.

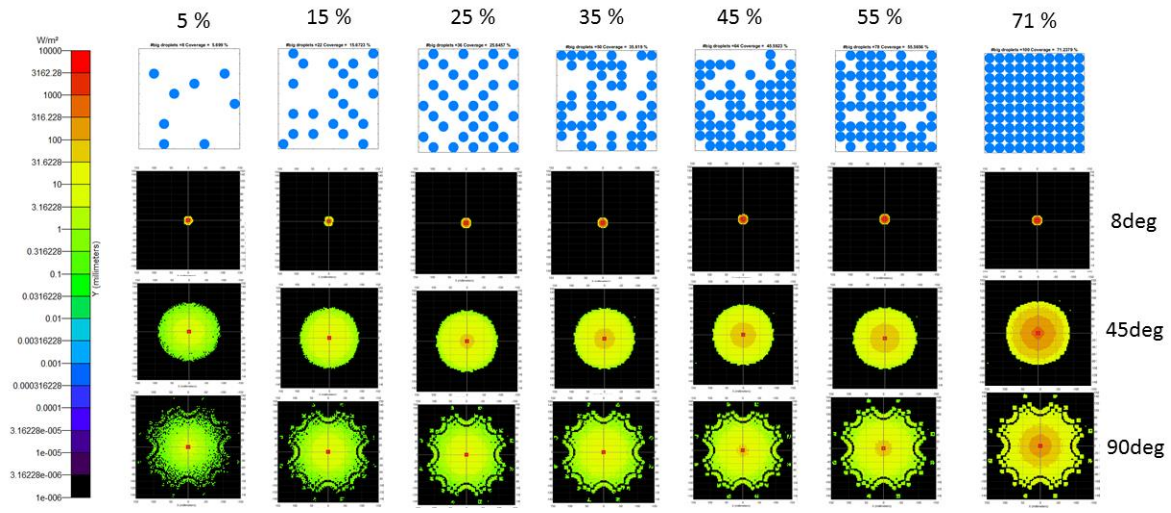

Figure 4.3. Simulation results for different coverage areas/contact angles

CHAPTER 5. FORMATION OF AN IMAGE WITH CONDENSATION

5.1 Dropwise Condensation

Water condensation is the change of water from its gas phase into a liquid phase. This process is initiated by a temperature differential between the vapor and the solid surface (glass substrate in our case). This study focused on heterogeneous condensation, which is a class of condensation that is divided into volume type and surface type. On one hand, volume condensation takes place in a region of space. Fog and mist clouds are a few example of this type. On the other hand, surface condensation takes place on a cooled surface near the water vapor. As the temperature of the surrounding environment drops, the water particles move close enough to start forming a cluster at specific sites at the atomic-scale (contaminant nuclei). These clusters will grow as more water is collected from the surrounding vapor. Once they reach a size where the separating distance between nearby droplets is equal or less the droplets diameter [8], the coalescence phase starts producing larger droplets and clears some of the substrate area that was previously covered. Clustering will occur in the newly cleared area and the cycle will be repeated.

As the droplet grows, its contact angle will depend on thermal, physical and chemical properties of the substrate as well as the vapor. As shown in Figure 5.1 (left), as the contact angle increases the wettability decreases and vice-versa. In a surface with

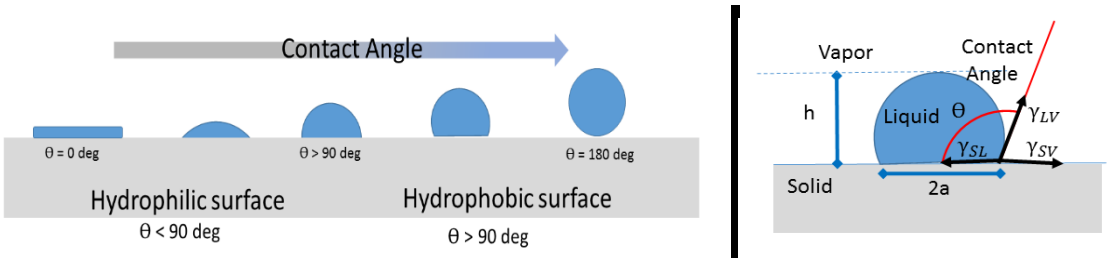

Figure 5.1. Wetting a surface

complete wetting, the condensation will take on the form of a film while in a non-wet surface the droplets will take on the form of water beads. Young's equation relates the different surface tensions applied to the droplet with the contact angle:

$$\gamma_{SL} = \gamma_{SV}.\text{COS}\theta + \gamma_{LV} \quad (1)$$

Where: γ_{LV} is the liquid surface tension,

γ_{SV} is the solid surface tension,

γ_{SL} is the liquid-surface interfacial tension, and

θ is the contact angle.

5.2 Modelling Condensation Effect

5.2.1 Geometrical Optics

A light point source **S** will emit a spherical wave front. This wave will diverge in space with rays radiating radially outward from the source. When a converging optical element (lens) is encountered the diverging wave front will collapse to a point **P**; however, when the point source is far away from the optical element the curvatuer of the wave front, it becomes negligeable and it is safe to assume that the wave front is a plane instead with light rays parallel to each other.

For an optical element (thin lens) with a diameter **D** located at a distance **s** from the source, if this lens have a positive focal length **f** then the light rays will converge to an image point located at a distance **i** from the lens. These three distances are related by a mathematical equation that describes the imaging system:

$$\frac{1}{s} + \frac{1}{i} = \frac{1}{f} \quad (2)$$

When the light ray hit the lens with an angle of **Θ** to the normal of the surface lens, the incident light can undergoes a refraction, reflection or both (Figure 5.2). The direction of the light ray before and after going through the optical element is captured by Fresnel's equation for reflection and transmission:

$$n_1 \sin\theta_1 = n_2 \sin\theta_2 \tag{3}$$

For a plano convex lens with an index of refraction n and that of the air is 1, if small angles are assumed, Snell's equation can be simplified by the following approximation:

$$n\theta_1 \backsimeq \theta_2 \tag{4}$$

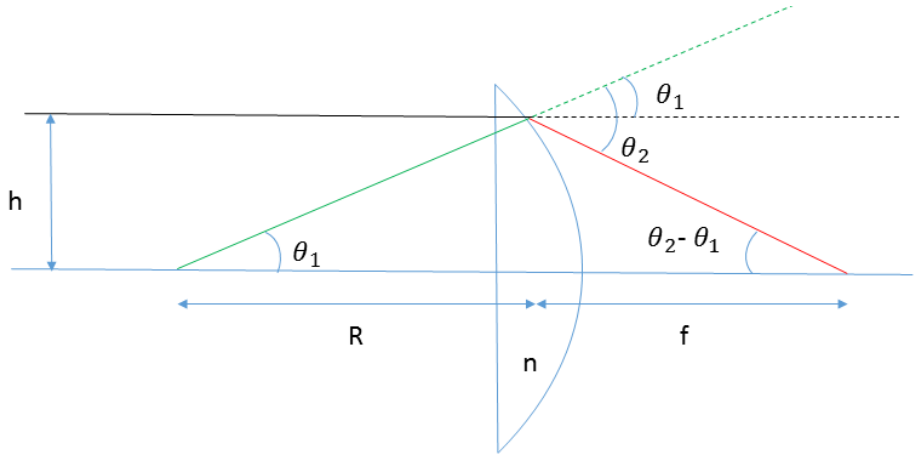

Figure 5.2. Ray tracing a beam in a plano convex lens

The difference between the incendent and refracted rays is substituted, resulting in:

$$\theta_2 - \theta_1 = (n-1)\,\theta_1 = \tan(\theta_2 - \theta_1) = \frac{h}{f} \tag{5}$$

The following approximation is applied for the incident ray:

$$\theta_1 = \frac{h}{R} \tag{6}$$

Using equations (2), (4) and (6) are then expressed as:

$$\frac{1}{f} = \frac{1}{s} + \frac{1}{i} = \frac{n-1}{R} \tag{7}$$

A thin lens can be described as a two plano convex lens that are placed with the flat sides in contact. Similiarly an equation that describes the second plano convex lens is:

$$\frac{1}{s_{sd}} + \frac{1}{i_{sd}} = \frac{n_{sd}-1}{R_{sd}} \tag{8}$$

The image for the first plano convex lens is the source for the second plano convex lens, hence:

$$s_{sd} = - i \tag{9}$$

Combining equation (7), (8) and (9) forms the Lens Maker's Equation which defines the relationship between the focal distance, the lens index of refraction and the radii of both cenvex sides:

$$\frac{1}{f_{lens}} = (n_{lens} - 1)(\frac{1}{R_1} + \frac{1}{R_2}) \tag{10}$$

5.2.2 Out-Of-Focus Kernel

Image blur is a form of degradation of the original viewed scene that results in a loss of image information (e.g. high frequencies). This generally takes place when the vision system used to capture the image is Out-Of-Focus or when in motion. The current work addressed the Out-Of-Focus case since it does contribute to the formation of an image with condensation build-up.

An Out-Of-Focus image can be modeled as the convolution of the perfect image with a blur kernel which in this case is the vision system point spread function (PSF):

$$I_{r,c}^{blurry} = K_{r,c} * I_{r,c} + W_{r,c} \tag{11}$$

Where: $I_{r,c}^{blurry}$ is the blurry image,

$K_{r,c}$ the blur kernel,

$I_{r,c}$ is the undistored original image,

$W_{r,c}$ is the image noise, and

* means convolution.

The PSF for a perfect optical system where a circular element is used (lens) can be modeled as an Airy Pattern [9]:

$$K_n = \frac{1}{(1-\varepsilon^2)^2}\left[\frac{2J_1(n)}{n} - \varepsilon^2 \frac{2J_1(\varepsilon n)}{\varepsilon n}\right]^2 \quad (12)$$

Where: ε is the aperture radius,

n is the distance from the optical axis in the focal plane, and

J_1 is the first order Bessel function.

The Airy Pattern model is rarely used due to its complexity; instead, a more simplified approximation is used. One of the widely used model is the Gaussian function:

$$K_{r,c} = \frac{1}{\sqrt{2\pi}\sigma}\exp\left(-\frac{x^2+y^2}{2\sigma^2}\right) \quad (13)$$

where σ is the spread parameter.

Nevertheless, the most common and efficient model for the Out-Of-Focus blur kernel is given by the mathematical expression:

$$K_{r,c} = \begin{cases} \frac{1}{\pi D^2} & if\ (r-k)^2 + (c-l)^2 \leq D^2 \\ 0 & elsewhere \end{cases} \quad (14)$$

where D is the radius of the kernel, and (k,l) is the kernel center location.

When the Vision System is in focus, no blur will be apparent and the image will be captured perfectly. In this case, the kernel can be modeleled as a Dirac delta function:

$$K_{r,c} = \delta_{r,c} \tag{15}$$

A good Out-Of-Focus kernel should satisfy the following constraint:

$$\iint_{-\infty}^{+\infty} K_{r,c} dr dc = 1 \tag{16}$$

5.2.3 Two Lens System

A two lens system approach, taking the droplet as the first thin lens and the camera lens as the second lens of the optical system, can be used to derive an expression that relates the droplet size, contact angle and the diamter of the Circle-Of-Confusion (see Appendix-B-1, B-2 and B-3). A focal lenght of 8 mm, a lens aperture 4 mm, a distance from the glass window to the target (object) of 290 mm and a camera-lens to window glass distance of 270 mm were used. As shown in Figure 5.3, for a droplet with a large contact angle the diameter of the CoC does not change much as the droplet grows, but the change becomes more significant as the contact angles drops down toward 0.

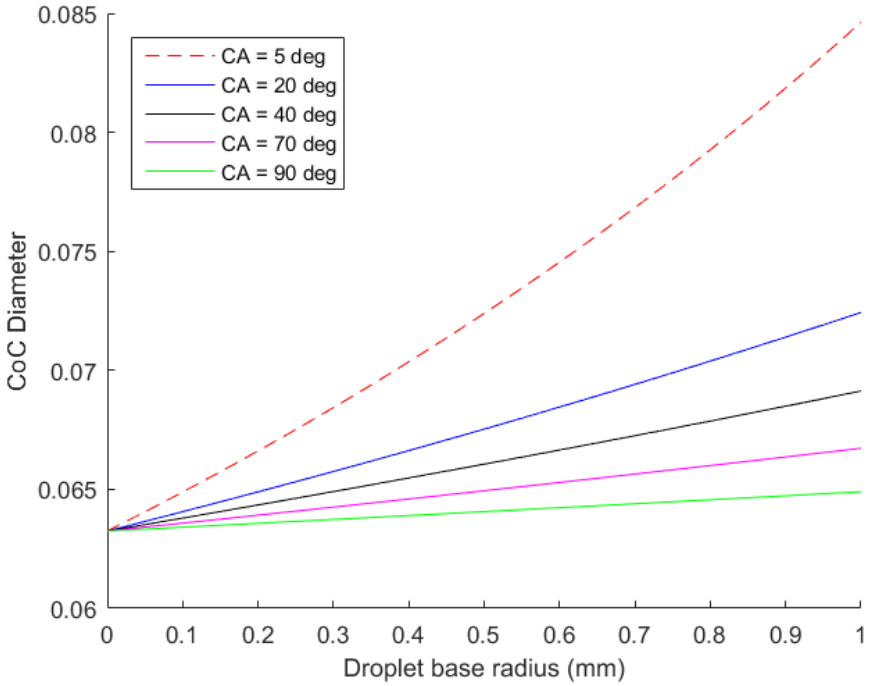

Figure. 5.3. Droplet base diameter vs. a CoC diameter

5.2.3 Models for Condensation Stages

The condensation process on a glass subtrate goes through multiple stages. After droplets form at the atomistic level (this phase was also covered in the section on Dropwise Condensation) [9], the growth stage begins where the droplets size increase from direct contact with vapor.

As the image starts getting foggy (growth phase), one can still distinguish the different colored squares of the checkerboard. This is because at this stage the droplets are too small and there is still enough clear area around each one to let considerable light reflected by the image to get through. As the density of the droplet increases, most of the scene region will be occluded by the droplets and the incoming light will be forced to go through the droplets instead (Figure 5.4, left bottom image).

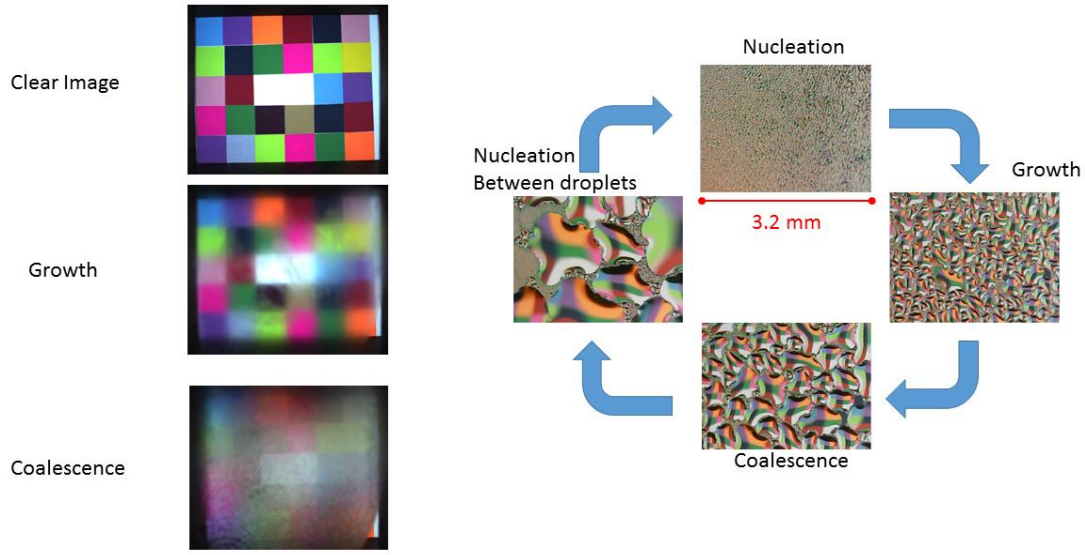

Figure 5.4. Dropwise condensation cycle

The apperance of the occluded region of the image will depend mainly on the geometry of the droplets. The larger the contact angle, the wider the droplet field of view; hence, each droplet will capture most of the scene. In this case if the portion of the image captured by the camera sensor pixel is much larger than the droplet diameter, then each

pixel will capture multiple droplets and the pixel intensity value will tend to be close to that of the average of the entire image. When a droplet reaches a certain size it starts to coalesce with neighbors to produce a bigger droplet. During this process the area previously occupied will be cleared and the nucleation will start all over again. The appearance of the occluded region of the image will depend mainly on the geometry and size of the droplets.

Case 1: Droplet size is much smaller than the pixel size:

The irradiance wich is the radiant falling on a surface can be expressed as follows:

$$E = \frac{I \cos\theta}{d^2} \quad \text{and} \quad E = \int_{\Omega} K_\theta \, L_i \mathrm{d}\omega \tag{17}$$

Where: I is the intensity, θ is the angle of incident,

d is the distance to the source,

L_i is the surface radiance, and

K_θ is a term with a dependency on the angle of incident.

Combining these two expressions results in:

$$I_{r,c} = \int_{\Omega} d^2 K_\theta \, L_i \mathrm{d}\omega \tag{18}$$

By using the intensity expression, one can formulate a model for the intensity of a point at (r, c) in the captured image:

$$I_{r,c}^{cond} = \alpha_{r,c} I_{r,c} + N(1 - \alpha_{r,c}) \frac{\pi R^2}{A^2} \int_{\Omega_{droplet}} d^2 K_\theta \, L_i \mathrm{d}\omega_{droplet} \tag{19}$$

Where: $\alpha_{r,c}$ is the fraction of the clear area,

$I_{r,c}^{cond}$ is the intensity of the curent pixel,

$I_{r,c}$ is the intensity of the pixel at (r,c) in the absence of any droplet,

R is the droplet radius,

A is the pixel area,

$\int_{\Omega_{droplet}} d^2 K_\theta \, L_i \mathrm{d}\omega_{droplet}$ is the intensity captured by the droplet image, and

N is the number of droplets within the pixel area.

In this formula it is assumed that all droplets are similar in size and shape, thus, it is apparent that the intensity of a pixel belonging to a condensation region will depend on the size, density and shape of the droplet (see Figure 5.5).

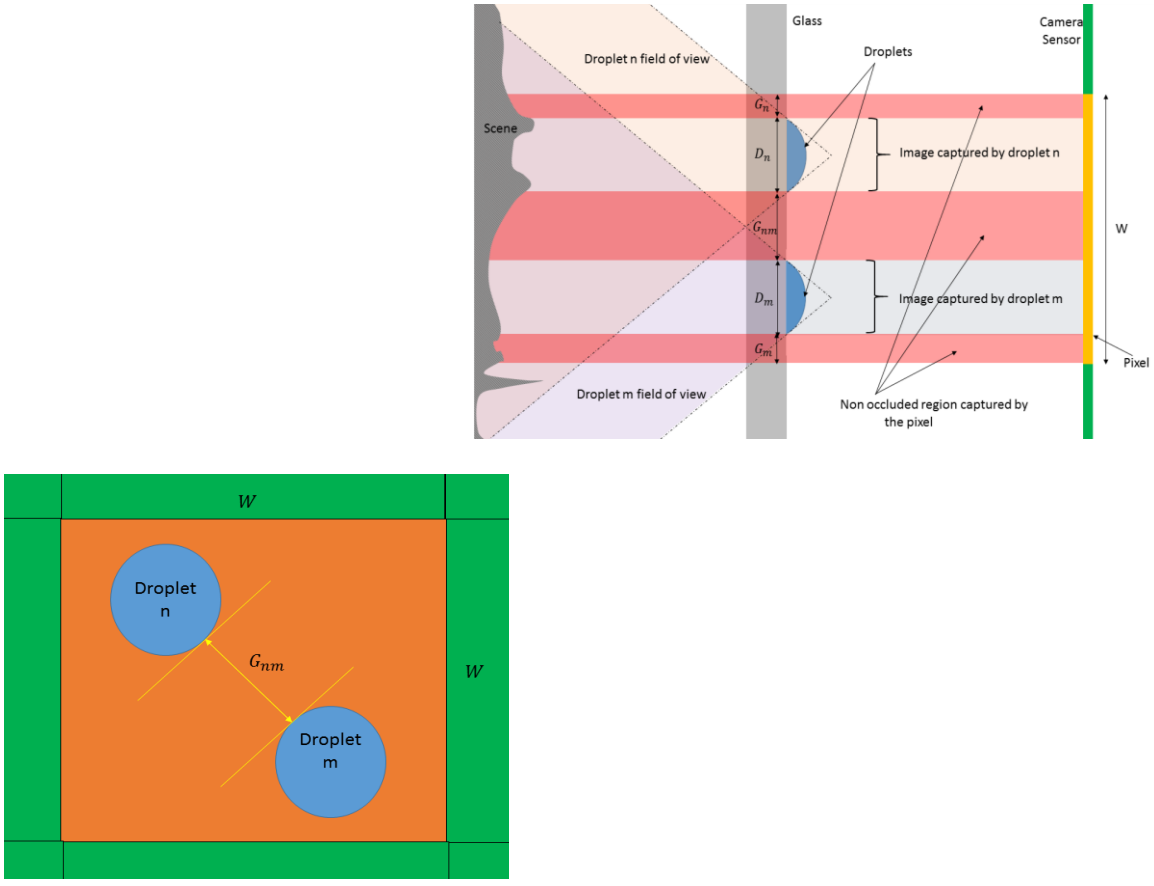

Figure 5.5. Occluded pixel area

As the droplets density increases, $\alpha_{r,c}$ will decrease and can get close to zero when the pixel area is totally packed with small droplets. These droples are close enough that it is safe to assume they are all capturing the same region of the scene.

If this region is with an intensity average of I_{avg}, then the pixel intensity will become:

$$I_{r,c}^{cond} = \alpha_{r,c} I_{r,c} + N(1 - \alpha_{r,c}) \frac{\pi R^2}{A} I_{avg} \sim I_{avg} \quad (20)$$

As the droplets contact angle get larger, the image contained by all droplets covering the glass substrate will be the same capturing the entier scene; thus, I_{avg} will become the image intensity average. On the other hand if the contact angle get so small (film of water) the condensation will have no effect, and $I_{r,c}^{cond} = I_{r,c}$.

Case 2: Droplet diameter is a few pixels

The same mechanism applies in this case. The image captured by each droplet will depend mainly on the contact angle; however, even though the droplet size is a few pixels, one cannot visually recognize the droplet, which is due mainly to downsampling. In this case a multi-focus model [11] must be used:

$$I_{r,c}^{cond} = p(\delta_{r,c} * I_{r,c}) + q(K_{r,c} * I_{r,c,droplets}) \quad (21)$$

Where: q is the droplet mask,

p is the complement mask of q,

$I_{r,c}$ is the clear image without droplets,

$K_{r,c}$ is the droplets blur kernel, and

$I_{r,c,droplets}$ is the image that contains the focused background as well as the focused droplets.

Thus each droplet in the image will contain a region of the image convolved with the blur kernel. This smooths the droplet imagelet and also includes information from the region surrounding the droplet (from the background image). It gets more significant as one gets closer to the edges of the droplet. Finally, the resulting droplet imaglet will be downsampled.

A zoomed image ROI is shown in Figure 5.6, where the left image illustrates the pixels and a mock-up of a few droplets capturing an area of the scene. The middle image shows an image where the camera is focused on the condensation plane. In the right image (a zoomed version), the droplets nearby resemble with each other.

Figure 5.6. Droplet with a diameter of a few pixels in width

Case 3: Droplet diameter much greater than the pixel size:

In case 3, the droplet appears more clearly in the image. It was not be covered in the current work as it has already been addressed in many publications.

CHAPTER 6. DATA ANALYSIS AND DETECTION ALGORITHM

In the previous chapters, a theoretical model was developed to help understand image formation in the presence of condensation (Models for Condensation Stages and The Two Lenses Approach). A ray tracing package was used to further clarify the phenomena of light transmission through a glass window with condensation build-up.

The following section discusses the data collected with the Fog-Lab and image processing techniques to find the most significant features that can help classify an image region as clear or foggy. An image is composed of two layers that are identified as:

- A background where the image is the in focus.
- A foreground that is similar to an overlay containing the occluded image region by the water droplets.

6.1 Data Analysis

6.1.1 Intensity

In the foreground, each pixel can be mapped to either another pixel or a region in the background that went through two levels of transformations (an OOF blur and a down-sampling process). The final value (appearance) of the pixel will depend on the size of the droplet, its shape, the droplet density and the background content.

Figure 6.1 illustrates the impact of the density of condensation on image formation, a target containing a small white square in the middle of a black non-reflective background is used to capture an image with condensation. The top row (from right to left) shows a region within the white rectangle that is captured with the microscope showing the droplets. Note that the dark area around the droplet is not due to total reflection at the edges (see Apendix-A) but is a portion of the dark background that is captured by the droplet as well. The midlle and far left images are images of the entire view with the camera focused on the glass and the backgournd.

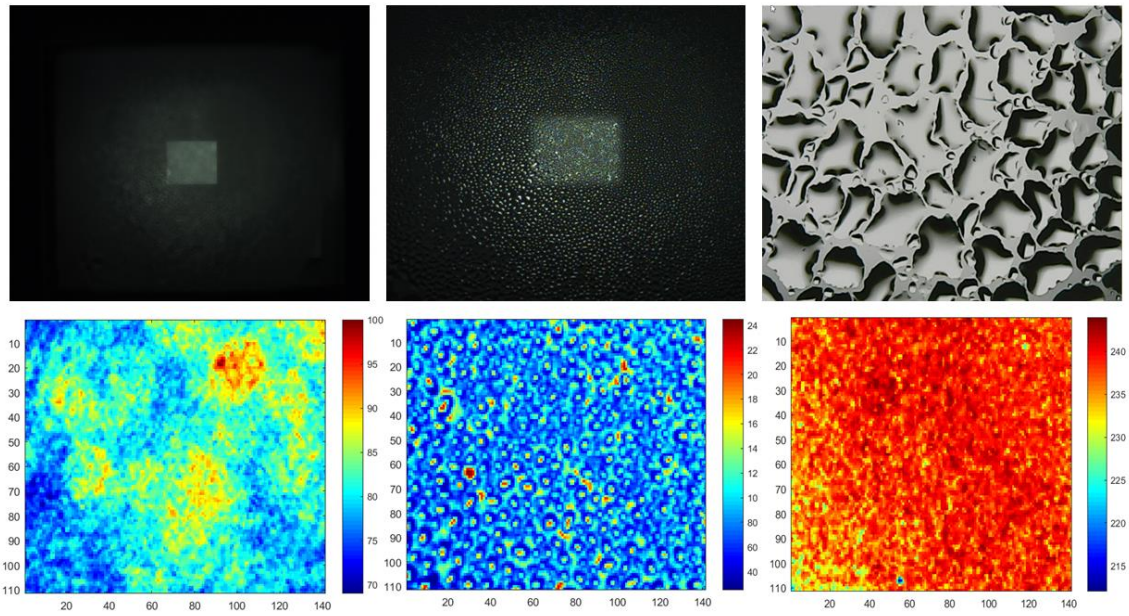

Figure 6.1. Intensity map for white/black target condensation

The second row illustrates an ROI of the white region. The right frame is the intensity map of a clear image (no condensation). The midlle one is the intensity map where the camera is focused on the glass. The intensity map on the left frame is that of an image focused on the background.

From these images, one can see that in regions with low droplets densisty, the background content will dominate. However in regions with high density, the pixel content will depend on the droplet contact angle. The latter case can be observed in the top-left image where dark spots appear within the white rectangle. This low intensity is caused by the fact that each droplet captued a portion of the dark background which in turn contributes to the low intensity value.

Similarly, a target was used with a larger white rectangle in a dark background (Figure 6.2). In this case, the condensation has less effect in the middle of the image (top-left image) where the droplets are far away from the dark background which means that the imaglet captured by each droplet does not conatain any portion of the background.

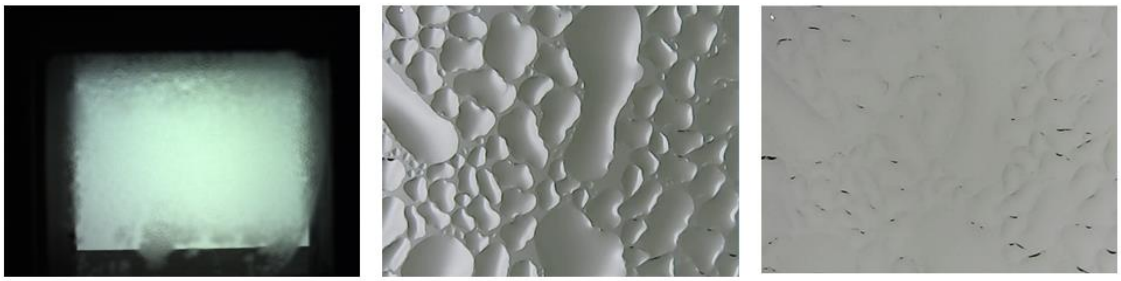

Fig. 6.2. Image with condensation using a large white target

However, as one gets closer to the edges of the white rectangle we can see that the intensity starts dropping to appear darker.

6.1.2 Chromaticity

Each pixel in the image quantifies the sum of a set of light rays reflected by a region within the scene. This process is modelled by the equation (17) that describes the interaction of the light from the source and the surface, hence the light reflected carries information about the surface it intercted with (material, color and orientation) as well as the intensity and direction [8]. Natural images usually capture surfaces with different orientations and colors, hence when assuming a labertian reflection and white illumination a colored surface will generate elongated streaks in the RGB color space [6].

In the presence of condensation, occluded pixels will contain information of a bigger ROI from the scene. In the case of droplets with small size (a couple of pixels and less) the RGB values of the pixel will be closer to the average RGB values of the ROI captured by the droplet. Hence the distribution of the pixels in the RGB color space will tend to move toward the centroid of that ROI (Figure 6.3).

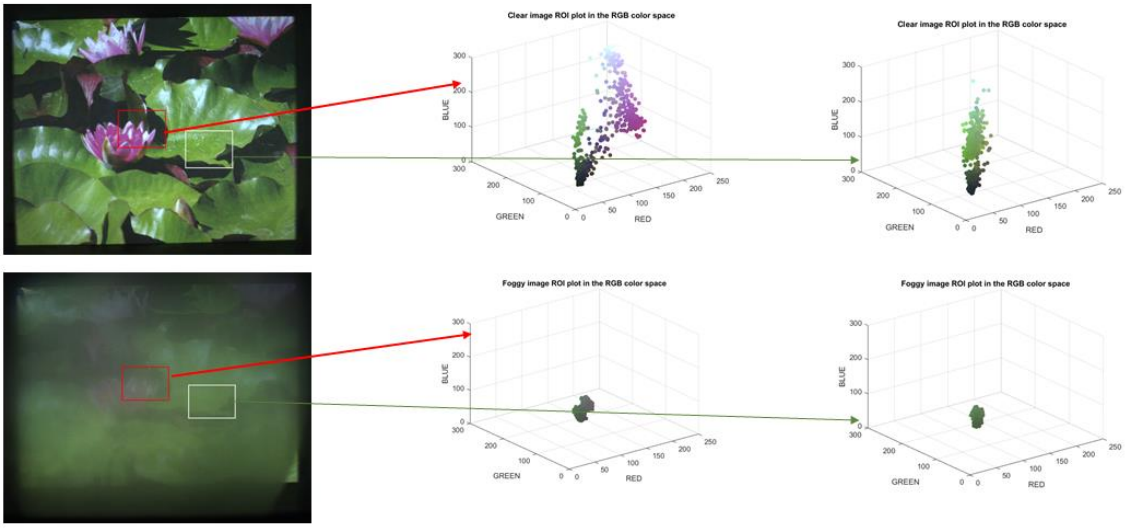

Figure 6.3. Pixel distribution in RGB space

The centroid of the ROI is computed to verify pixel formation in the RGB space:

$$r_{centroid} = \mu_R$$

$$g_{centroid} = \mu_G$$

$$b_{centroid} = \mu_B$$

Next, the Euclidian distance is computed from the centroid to all the other ROI pixels in the RGB color space. Thus, for a pixel k, the distance is:

$$d_{rgb}^{k} = \sqrt{(P_r - \mu_R)^2 + (P_g - \mu_G)^2 + (P_b - \mu_B)^2} \quad (22)$$

These distances from the centroid are used to calculate the variance for each selected patch (ROI):

$$\sigma^2 = \frac{\sum(d_{rgb}^{k} - \mu_d)^2}{N} \quad (23)$$

Using the mean of the Euclidian distances and the variance, the index of dispersion is computed next:

$$Index\ Of\ Dispersion = \frac{\sigma^2}{\mu_d} \quad (24)$$

This index is used to generate a color dispersion map by sliding a window with a predefined size over the entire image followed by a normalization. Figure 6.4 shows the dispersion map for three different images with different condensation coverage. The feature performed very well except in a few flat and dark regions:

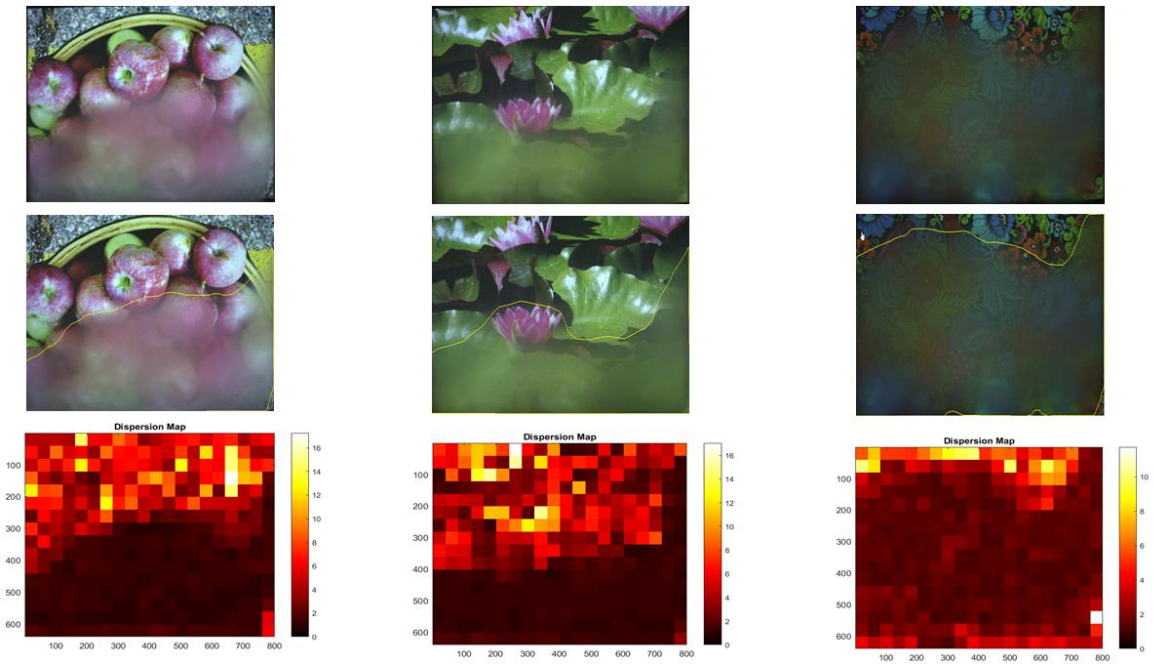

Figure 6.4. Dispersion map for three different condensation levels

As the condensation builds up, the dispersed pixels for each patch within the affected region will move toward the centroid taking the shape of an ellipsoid. The vector's azimuth and elevation distributions should be symmetrical for each centroid pixel vector. Hence, the skewness should be near zero. The azimuth skewness map is shown in Figure 6.5, and elevation sknewness map appears in Figure 6.6. In the same way, a skewness map is generated using the following metric where image patch is first shifted centroid to the origin of the RGB color space before calculating the elevation and azimuth:

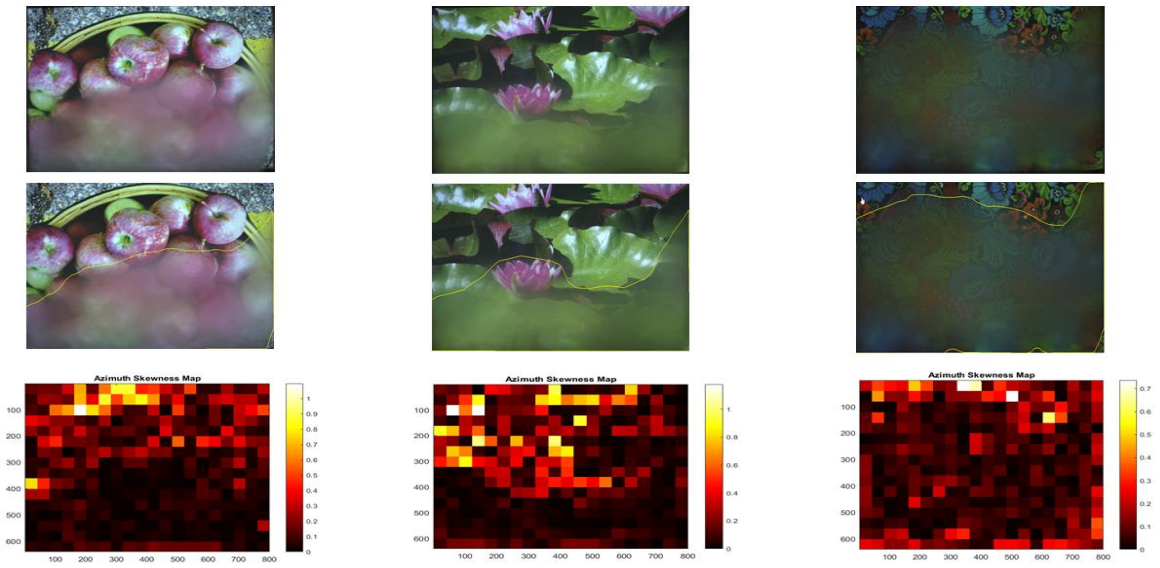

Figure 6.5 Azimuth skewness map

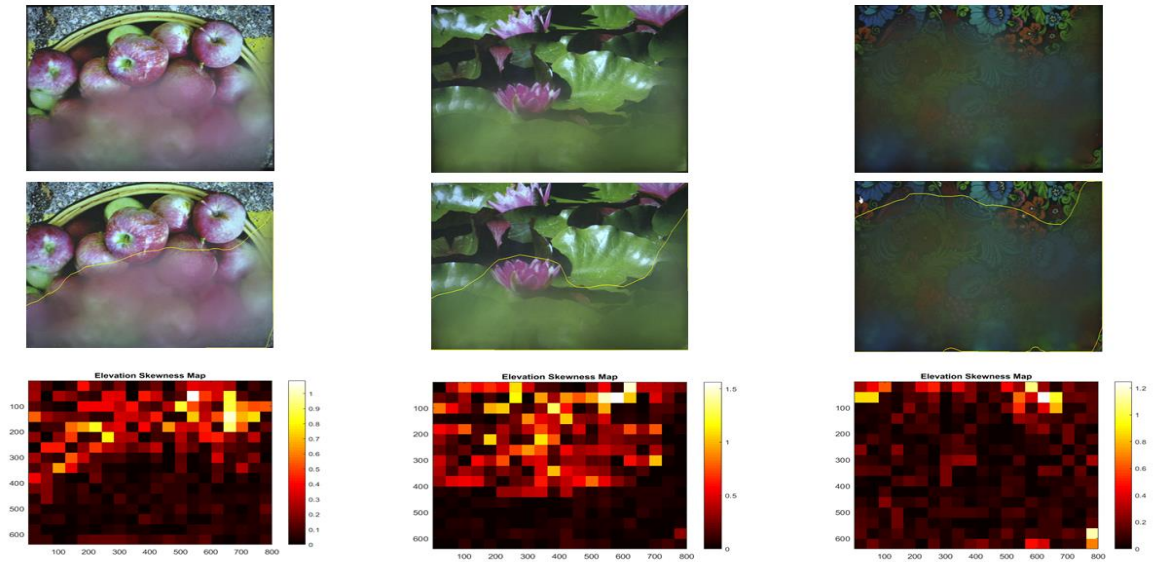

Figure 6.6. Elevation skewness map

$$Elevation\ Skeweness = \frac{E(P_{elevation} - \mu_{elevation})^3}{\sigma^3_{elevation}} \quad (25)$$

$$Azimuth\ Skeweness = \frac{E(P_{azimuth} - \mu_{azimuth})^3}{\sigma^3_{azimuth}}$$

When looking at the elevation and azimuth skewness maps, it is apparent that there are two distributions, and they match with the foggy and clear image regions. However, the map seems to be noisy which this is most likely due to the non-uniform droplet density. In order to verify this hypothesis, the Fog-Lab will require some updating to make the data collection more precise and eleminate evaporation especially at the early stages of condensation.

6.1.3 Texture

To investigate the effect of condensation on image texture, the first analysis is the Edges Orientation Histogram whereas the symmetrical image with a repetitive pattern is used as a target in this test. The idea is to compute the gradient orientation using Sobel Operators for a clear original image and then redo the same operation for different levels of condensation in ordere to evalute this feature.

The gradient is computed at 5 different oriontations for the Edges Orientation Histogram. Each one of these masks is convolved with the original mask to produce an image of the gradient for that specific orientation. A histogram is then plottedd for each one for three different levels of condensation.

$$\text{Horizontal Mask}: \begin{matrix} -1 & -2 & -1 \\ 0 & 0 & 0 \\ 1 & 2 & 1 \end{matrix}$$

$$\text{Vertical Mask}: \begin{matrix} -1 & 0 & 1 \\ -2 & 0 & 2 \\ -1 & 0 & 1 \end{matrix}$$

$$\text{Diagonal Mask}: \begin{matrix} -2 & -1 & 0 \\ -1 & 0 & 1 \\ 0 & 1 & 2 \end{matrix}$$

$$\text{Non}-\text{Directional Mask}: \begin{matrix} -1 & 2 & 2 \\ -1 & -1 & 2 \\ -1 & -1 & -1 \end{matrix} \quad \text{and} \quad \begin{matrix} -1 & 0 & 1 \\ 0 & 0 & 0 \\ 1 & 0 & -1 \end{matrix}$$

As shown in the histogram plots (Figure 6.7), as the condensation gets heavier the amount of change within the image (Texture) increases. This contradicts the research hypothesis. One explanation for this phenomenon could be that the target selected and used in this test is a high contrast/low texture density, which makes the presence of the droplets in the image scene – the new texture – offset the blending effect (blurriness) caused by the condensation.

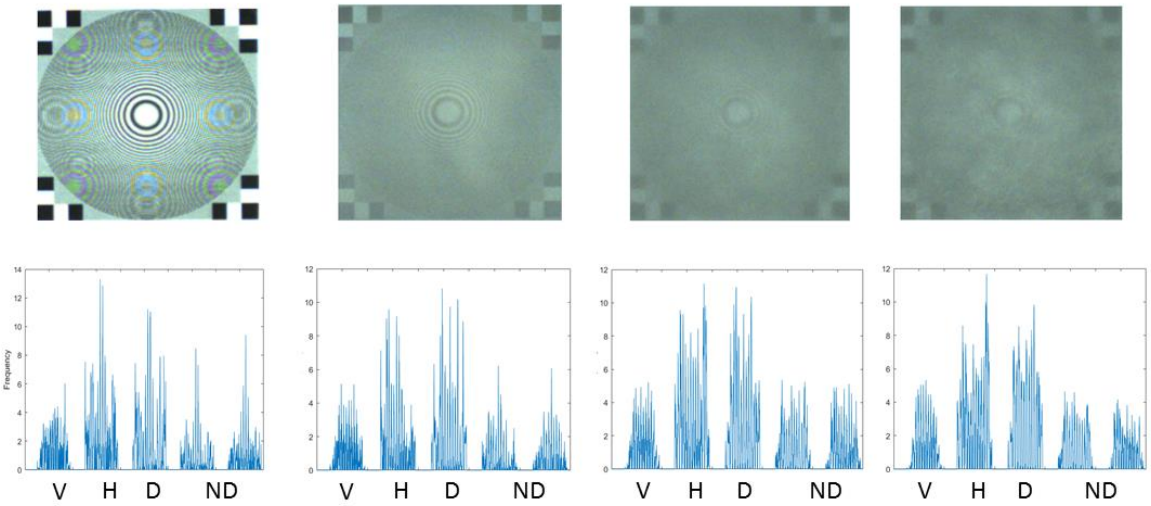

Figure 6.7. Edges histogram orientation for different condensation levels

The next test ignores the direction of the gradient and calculates the mean gradient magnitude [6]. A map is constructed by dividing the image with a grid and computing the gradient magnitude for each cell:

$$Image\ Cell\ Gradietn\ magnitude = \sqrt{(\frac{\partial I}{\partial x})^2 + (\frac{\partial I}{\partial y})^2} \qquad (26)$$

Figure 6.8 shows the maps generated with their corresponding images. The gradient magnitude feature performed very well isolating the two distributions (clear vs foggy). The main reason this worked is because the images used are natural images containing a higher texture spectrum, and these images are usually heavy-tailed ([2], [3], [4] and[10]). Thus, the gradient magnitude will have a high variance; however, as the

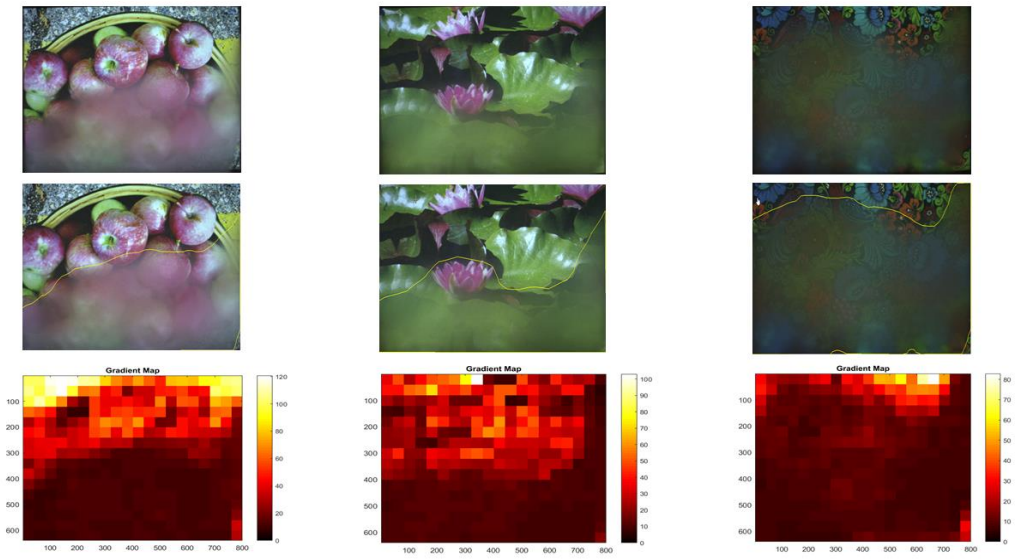

Figure 6.8. Gradient magniture map for different condensation levels

condensation start building up an out of focus overlay (in the case of small droplets with a higher density) will drive the gradient magnitude variance down, hence separating the foggy region distribution from that of the clear area.

6.2 Proposed Detection Algorithm

Now that a couple of reliable features have been identified, the image can be modeled as a Gaussian mixture model (GMM):

$$G_{Img} = \alpha_{Clear} e^{\frac{-(G_{Clear}-\mu_{Clear})^2}{\sigma_{Clear}}} + \alpha_{Foggy} e^{\frac{-(G_{Foggy}-\mu_{Foggy})^2}{\sigma_{Foggy}}} \quad (27)$$

First, the image is divided into a grid and for each cell, and the dispersion and gradient magnitude is computed. When plotting the two features, one can see that it contains two different Gaussian distributions; the more clustered one is for the foggy region while the rest is for the clear part. This actually verifies the image can be segmented reliabley into two clusters. An unsupervised classification is applied since the mean and variance of the two distributions can be different for each background. However, it is known that the variance for both features will be low for the foggy region (see Figure 6.9).

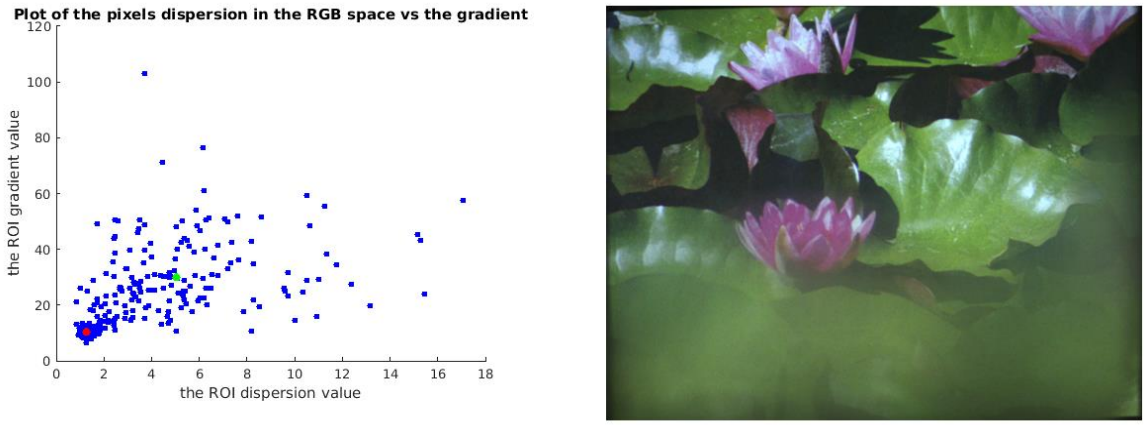

Figure 6.9. RGB dirpesion-gradient magniture scatter plot for foggy image

The Expectation Maximization algorithm is used to classify the image cells. Thus, for two clusters (k =2) for an image with a set of N×M data point X, let: C_{Clear} be the cluster for the clear image portion and C_{foggy} be the cluster for the foggy region

First, the mean and variance for both distributions are initialized with some arbitrary values. One can then compute the conditional probability for each data point to belong to either one of the two clusters. This step indicates that, with the current clear and foggy distribution parameters, whether or not the selected data point (in this case an image cell) looks like it is affected by condensation using a soft segmentation. Next, the computed probabilities are used to update the distributions parameters (a maximization problem).

Once the iterative process is completed, it results in two segments (clear and foggy). Then one more pass can be made to find outlier cells where a clear cell is surrounded by foggy ones. A final clustering decision for the questioned outlier is based on the probability of the neighboring cells to belong to the foggy segment as well as the cell dominant color (Figure 6.10).

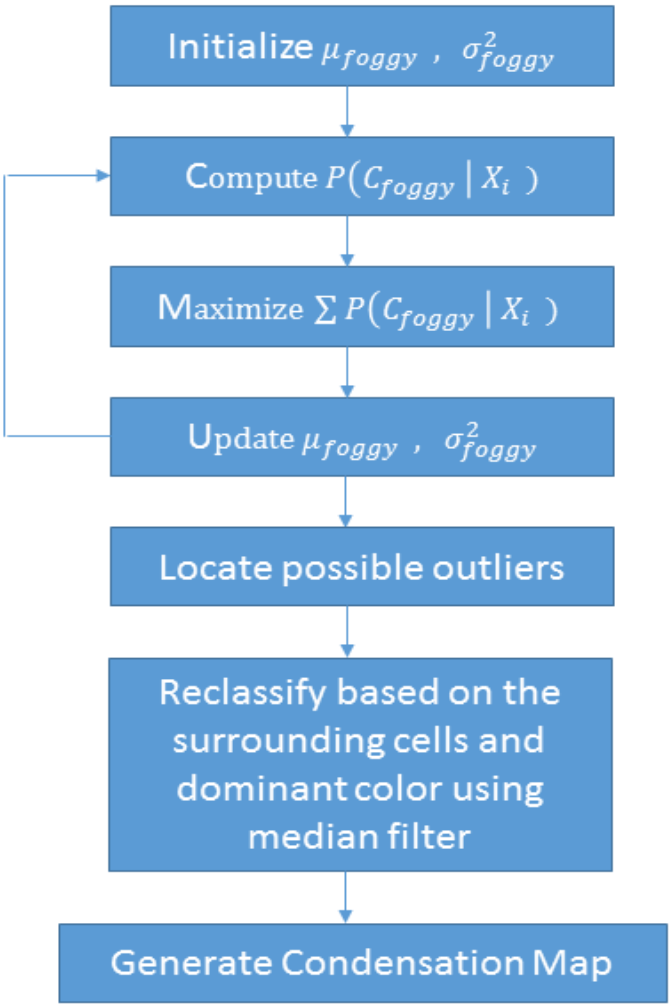

Figure 6.10. Dispersion-Gradient detection agorithm block diagram

Figure 6.11 illustrates the results from the unsupervised classification where the value of each cell in the map is the probability that the cell belongs to a clear image region. The classification works well when dealing with natural images or with enough texture but will fail if the image is flat as the impact of condensation will be insignificant due to the low pixels dispersion in the RGB color and low texture space.

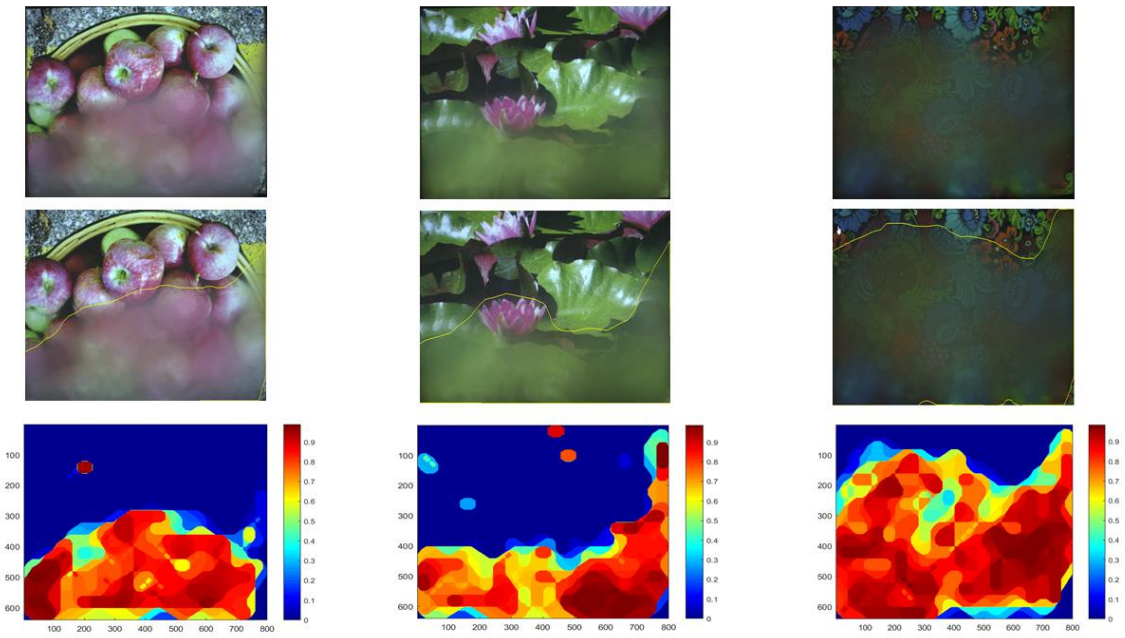

Figure 6.11. Dispersion-Gradient clustering map

6.3 Detection Method in the Luminance-Chrominance Space

This section investigates the structre of the pixels distribution in the Luminance-Chrominance space using the Lab color space. As shown in Figure 6.12, condensation produces multiple parallel clusters in the a|L scatter plot (a: the horizontal axis represents the pixel chrominance; and L: the vertical axis represents the pixel luminance). As the condensation gets heavier the clusters shift downward which makes sense since the image gets darker.

The clustering feature in the a-L space can be used to classify the regions in the image as clear or foggy. First, the image from the RGB is converted to Lab color space, and then it is scanned through the image using a sliding window. This enables the construction of an a|L scatter (Figure 6.13). The entire image is transformed to find the dominant line slope, which enables one to cluster pixels using the slope. After completion, a fraction of clustered pixels are used to classify whether or not the cell is foggy.

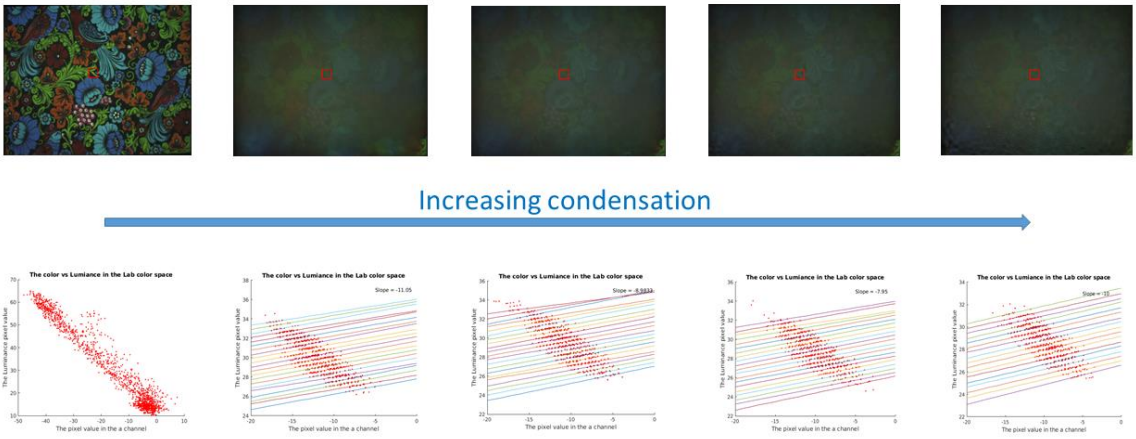

Figure 6.12. Clustering in the Luminance-Chrominance space

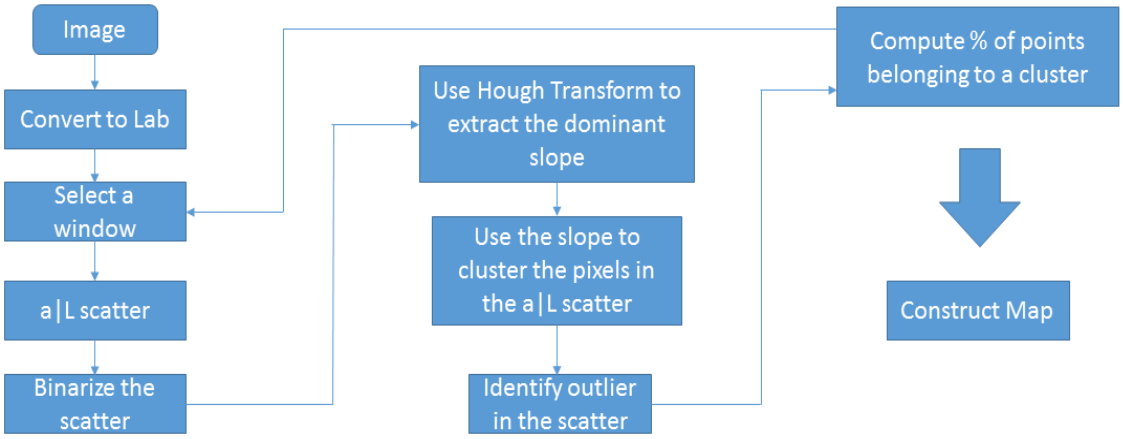

Figure 6.13. Clustring in the Luminance-Chrominance algorithm block diagram

CHAPTER 7. CONCLUSION AND FUTURE RESEARCH

Detecting condensation is a very challenging problem, since it cannot be treated as a blur model. If the droplet is large enough, some generic texture and chromatic features can be used to generate a classifier or a filter that captures the droplet effect. On one hand, simply training a classifier using many images with droplets will depend heavily on the captured scenes within the data used and may fail when testing it with different data sets (e.g. training a classifier with droplet capturing the sky and testing it with a data set where the images do not contain the sky). On the other hand, no template can be generated when the droplets are not large enough as in this case. However, a model can be generated that reflects the effect of many droplets on a single pixel or a small image patch should be used.

The work presented in this thesis research introduced a method for detecting water condensation in a single image where the droplets size is a couple of pixels at most. This approach is unique as it segments an image into clear and foggy regions where water droplets are not visually distinguishable within the image. The solution developed in this work is fundamental to the monitoring of image quality in a computer vision system where the detection can be used to either discard foggy regions from the image processing/classification logic or trigger a warning to clean the camera window or lens.

The algorithm that was developed in this research was verified using data collected from a Fog-Lab in a controlled environment. This procedure ensured that the light reflected by the scene and captured by the image sensor was constant while only varying the level of condensation build-up in the camera's field of view. The data and grounded truths (macroscopic as well as microscopic) will be beneficial to future research in the field. In the future, this Experimental set-up (Fog-Lab) could be modified to eliminate droplet evaporation at the early stages of the condensation for continued

algorithm verification and development. Currently, the glass is exposed to room temperature which makes the data collection very difficult for certain stages.

REFERENCES

[1] Liu, R., Li, Z., & Jia, J. (2008). Image partial blur detection and classification. *2008 IEEE Conference on Computer Vision and Pattern Recognition*. doi:10.1109/cvpr.2008.4587465

[2] Chen, M., & Bovik, A. C. (2009). No-reference image blur assessment using multiscale gradient. *2009 International Workshop on Quality of Multimedia Experience.* doi:10.1109/qomex.2009.5246973

[3] Shi, J., Xu, L., & Jia, J. (2014). Discriminative Blur Detection Features. *2014 IEEE Conference on Computer Vision and Pattern Recognition.* doi:10.1109/cvpr.2014.379

[4] Yi, X., & Eramian, M. (2016). LBP-Based Segmentation of Defocus Blur. *IEEE Transactions on Image Processing*, *25*(4), 1626-1638. doi:10.1109/tip.2016.2528042

[5] Bahrami, K., Kot, A. C., & Fan, J. (2013). A novel approach for partial blur detection and segmentation. *2013 IEEE International Conference on Multimedia and Expo (ICME)*. doi:10.1109/icme.2013.6607493

[6] Gevers, T. (2012). *Color in computer vision: fundamentals and applications.* Hoboken, NJ: Wiley.

[7] Theodoridis, S., & Koutroumbas, K. (2010). *Introduction to pattern recognition a MATLAB approach.* Burlington, MA: Academic Press.

[8] Pouli, T., Cunningham, D. W., & Reinhard, E. (2014). *Image statistics in visual computing.* Boca Raton, FL: CRC Press/Taylor & Francis Group.

[9] Khandekar, S., & Muralidhar, K. (2014). *Dropwise condensation on inclined textured surfaces.* New York, NY: Springer New York.

[10] Roth, S., & Black, M. (n.d.). Fields of Experts: A Framework for Learning Image Priors. *2005 IEEE Computer Society Conference on Computer Vision and Pattern Recognition* (CVPR05). doi:10.1109/cvpr.2005.160

[11] Dai, S., & Wu, Y. (2009). Removing partial blur in a single image. *2009 IEEE Conference on Computer Vision and Pattern Recognition*. doi:10.1109/cvprw.2009.5206625

[12] Ito, K., Noro, K., & Aoki, T. (2015). An adherent raindrop detection method using MSER. *2015 Asia-Pacific Signal and Information Processing Association Annual Summit and Conference (APSIPA)*. doi:10.1109/apsipa.2015.7415468

[13] Sugimoto, M., Kakiuchi, N., Ozaki, N., & Sugawara, R. (2012). A novel technique for raindrop detection on a car windshield using geometric-photometric model. *2012 15th International IEEE Conference on Intelligent Transportation Systems*. doi:10.1109/itsc.2012.6338613

[14] Roser, M., & Geiger, A. (2009). Video-based raindrop detection for improved image registration. *2009 IEEE 12th International Conference on Computer Vision Workshops, ICCV Workshops*. doi:10.1109/iccvw.2009.5457650

[15] Wu, Q., Zhang, W., & Kumar, B. V. (2012). Raindrop detection and removal using salient visual features. *2012 19th IEEE International Conference on Image Processing*. doi:10.1109/icip.2012.6467016

[16] Webster, D. D., & Breckon, T. P. (2015). Improved raindrop detection using combined shape and saliency descriptors with scene context isolation. *2015 IEEE International Conference on Image Processing (ICIP)*. doi:10.1109/icip.2015.7351633

[17] Machot, F. A., Ali, M., Mosa, A. H., Schwarzlmüller, C., Gutmann, M., & Kyamakya, K. (2016). Real-time raindrop detection based on cellular neural networks for ADAS. *Journal of Real-Time Image Processing*. doi:10.1007/s11554-016-0569-z

[18] Eigen, D., Krishnan, D., & Fergus, R. (2013). Restoring an Image Taken through a Window Covered with Dirt or Rain. *2013 IEEE International Conference on Computer Vision*. doi:10.1109/iccv.2013.84

[19] Halimeh, J. C., & Roser, M. (2009). Raindrop detection on car windshields using geometric-photometric environment construction and intensity-based correlation. *2009 IEEE Intelligent Vehicles Symposium*. doi:10.1109/ivs.2009.5164347

[20] Kurihata, H., Takahashi, T., Ide, I., Mekada, Y., Murase, H., Tamatsu, Y., & Miyahara, T. (2005). Rainy weather recognition from in-vehicle camera images for driver assistance. *IEEE Proceedings. Intelligent Vehicles Symposium, 2005.* doi:10.1109/ivs.2005.1505103

[21] You, S., Tan, R. T., Kawakami, R., & Ikeuchi, K. (2013). Adherent Raindrop Detection and Removal in Video. *2013 IEEE Conference on Computer Vision and Pattern Recognition*. doi:10.1109/cvpr.2013.138

[22] Nashashibi, F., Charrette, R. D., & Lia, A. (2010). Detection of unfocused raindrops on a windscreen using low level image processing. *2010 11th International Conference on Control Automation Robotics & Vision*. doi:10.1109/icarcv.2010.5707398

APPENDIX A. GEOMETRIC-PHOTOMETRIC MODEL OF THE DROPLET

In this section we will derive an expression that relates the droplet contact angle and the reflectance

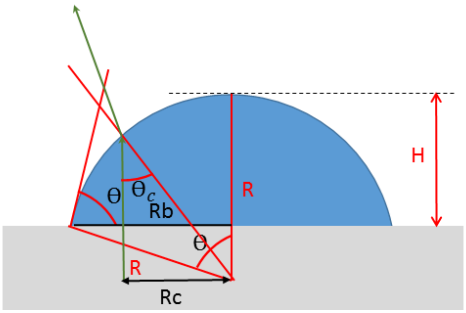

Figure A-1. Photometric model of the droplet

where θ is the contact angle, n_{drop} is the droplet index of reflecion(water), n_{air} is the air index of reflecion, R is the droplet radius, Rb is the droplet base radius, H is the droplet hight, Θ_c is the droplet critial contact angle (contact angle at wich we get total reflection).

When a ray traversing the droplet from the base hits the droplet-air interface with an angle of Θ_{drop} it will refract exiting the droplet with an angle of Θ_{air} (both angles here are in reference to the normal to the droplet surface at the point of exit), now we use Snell's Law:

$$n_{drop}\text{SIN}\Theta_{drop} = n_{air}\text{SIN}\Theta_{air} \tag{28}$$

We know that n_{drop} = 1.33 and n_{air} = 1; so, at the threshold angle for total internal reflection:

$$\Theta_{air} = 90\text{deg} \quad \text{thus} \quad \Theta_c = 48.75\text{deg} \tag{29}$$

As shown in Figure A-1, in the triangle defined by the critical base radius Rc and the droplet radius R:

$$\text{Rc} = \text{R*SIN}\Theta_c \tag{30}$$

In the triangle defined by the droplet radius R and droplet base radius Rb:

$$Rb = R*SIN\theta \tag{31}$$

Thus, the reflectance is:

$$1- \frac{\pi {R_c}^2}{\pi {R_b}^2} = 1- \frac{R*SIN\theta_c}{R*SIN\theta} = 1- \frac{SIN(48.75)}{SIN\theta} \tag{32}$$

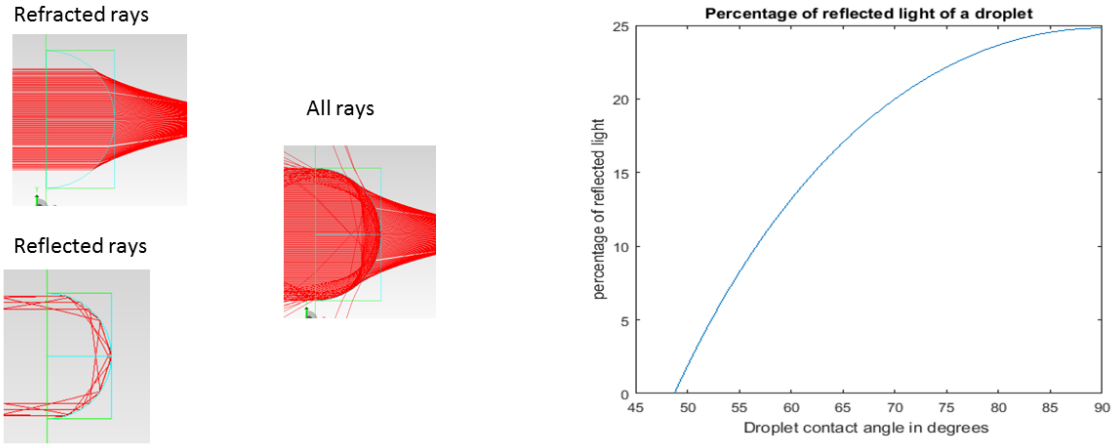

Figure A-2. Losses due to reflection

The plot in Figure A-2 (right) shows the reflectance vs the droplet contact angle for a range of [0-90 deg]. The left images are of a simulation using TracePro showing the reflected rays at the edges of the droplet.

APPENDIX B. GEOMETRIC-PHOTOMETRIC MODEL OF THE DOPLET-LENS MODEL

In this example, we will derive a expression that relates the droplet shape and size to the camera params and camera-condensation glass distance.

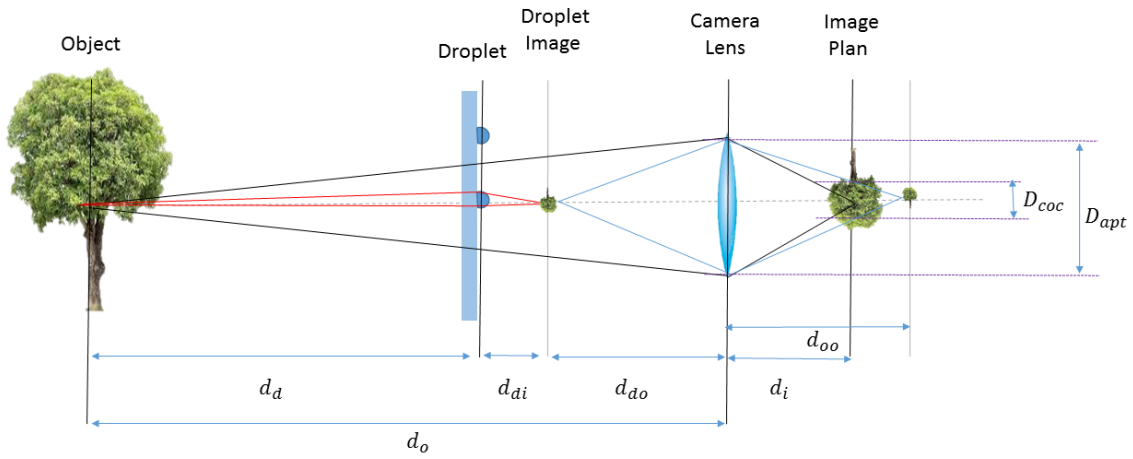

KEY:

$D_{droplet}$	droplet diameter
D_{apt}	lens aperture
D_{CoC}	diameter of the Circle of Confusion
D_d	distance from the object to the droplet
D_o	distance from the object to the camera lens
D_{di}	distance from the droplet to the droplet image
D_i	distance from the camera lens to the image
D_{do}	distance from the droplet image to the camera lens
D_{oo}	distance from the camera lens the image of the droplet image

Figure B-1. Ray tracing for a droplet-camera lens optical system

Using the first optical system (object-droplet) and setting the second radius (droplet flat side R_2) to infinity will get:

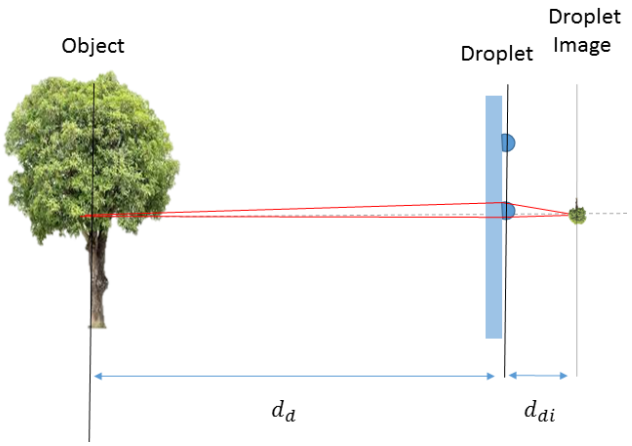

Figure. B-2. Ray tracing for a single droplet

$$\frac{1}{d_d} + \frac{1}{d_{di}} = \frac{1}{f_{droplet}} \quad \text{and} \quad \frac{1}{f_{droplet}} = (n_{water} - 1)\left(\frac{1}{R_{droplet}}\right) \tag{33}$$

and combining both equations we get:

$$d_{di} = \frac{R_{droplet} d_d}{d_d\,(n_{water} - 1) - R_{droplet}} \tag{34}$$

Now the virtual image focused by the droplet will serve as a source to the second optical system (camera), using again Snell's Law we get:

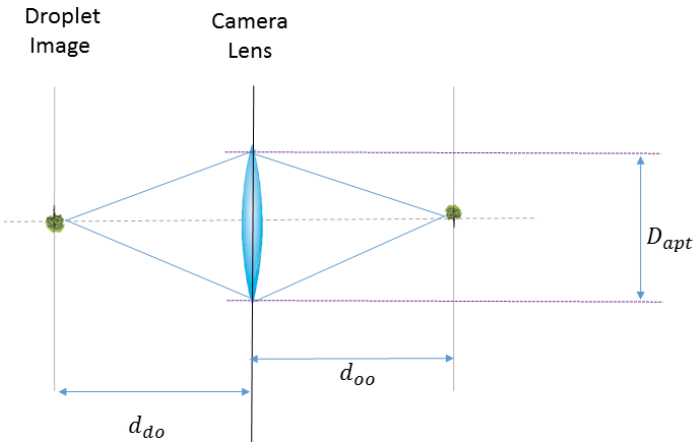

Figure. B-3 Ray tracing for a thin converging lens

$$\frac{1}{d_{do}} + \frac{1}{d_{oo}} = \frac{1}{f_{lens}} \text{ is equal to } d_{oo} = \frac{f_{lens}\, d_{do}}{d_{do} - f_{lens}} \tag{35}$$

Next we will use Snell's Law for the camera optical system capturing the scene (see Figure B-1):

$$\frac{1}{d_o} + \frac{1}{d_i} = \frac{1}{f_{lens}} \text{ is equal to } d_i = \frac{f_{lens}\, d_o}{d_o - f_{lens}} \tag{36}$$

We know also that the Circle-Of-Confusion and depth of field are related by the folowing equation:

$$\frac{D_{coc}}{d_{apt}} = \frac{d_{oo} - d_i}{d_i} = \frac{d_{oo}}{d_i} - 1 = \left(\frac{f_{lens}\, d_{do}}{d_{do} - f_{lens}}\right).\left(\frac{d_o - f_{lens}}{f_{lens}\, d_o}\right) - 1 \tag{37}$$

We then substitute d_{do} by $d_0 - d_d - d_{di}$:

$$\frac{D_{coc}}{d_{apt}} = \frac{(d_0 - d_d - d_{di})\,(d_o - f_{lens})}{d_o(d_0 - d_d - d_{di} - f_{lens})} - 1 \tag{38}$$

In addition, we know (from Apendix-A) that:

$$R_{droplet} = \frac{R_b}{\text{SIN}\theta} \tag{39}$$

Thus, equation (34) becomes:

$$d_{di} = \frac{R_{droplet} d_d}{d_d\,(n_{water} - 1) - R_{droplet}} = \frac{R_b d_d}{d_d\,(n_{water} - 1)\text{SIN}\theta - R_b} \tag{40}$$